

# Modeling Encounters of Galaxies: The Case of NGC4449

CHRISTIAN THEIS

*Institut für Theoretische Physik und Astrophysik, Universität Kiel, 24098 Kiel,  
Germany, email: theis@astrophysik.uni-kiel.de*

## Abstract

Several N-body methods were combined in order to develop a method for the determination of the parameters of interacting galaxies. This method has been applied to the HI distribution of NGC4449. In a first step the fast restricted N-body models were used to confine a region in parameter space reproducing the main observational features. In a second step a genetic algorithm is introduced which allows for an automated search in the high-dimensional parameter space as well as for a uniqueness test of special parameter sets. Using artificial data I show that the genetic algorithm reliably recovers orbital parameters, provided that the data are sufficiently accurate, i.e. all the key features are included. In the third step the results of the restricted N-body models are compared with detailed self-consistent N-body simulations. In the case of NGC4449 the applicability of the simple restricted N-body calculations is demonstrated. Additionally, it is shown that the HI gas can be modeled here without any restrictions by a purely stellar dynamical approach.

NGC4449 is an active star-forming dwarf galaxy of Magellanic type. From radio observations van Woerden et al. (1975) found an extended HI-halo around NGC4449 which is at least a factor of 10 larger than the optical diameter  $D_{25} \approx 5.6$  kpc. More recently, Bajaja et al. (1994) and Hunter et al. (1998) discerned details in the HI-halo: a disc-like feature around the center of NGC4449 and a lopsided arm structure. In a series of simulations it is demonstrated that the main features can be obtained by a gravitational interaction between NGC4449 and another nearby dwarf galaxy, DDO125. According to these calculations the closest approach between both galaxies happened  $\sim 3.5 \cdot 10^8$  yr ago at a minimum distance of  $\sim 25$  kpc on a nearly parabolic orbit. In case of an encounter scenario, the dynamical mass of DDO125 should not be smaller than 10% of NGC4449's mass. Before the encounter the observed HI was arranged in a disc with a radius of 35–40 kpc around the center of NGC4449 which had the same orientation as the central ellipsoidal HI structure. The origin of this disc is still unclear, but it might be caused by a previous interaction.

## 1 Introduction

During the last decades our picture of galaxies being 'Welteninseln' (e.g. Kant, 1755), i.e. island universes, has completely changed. At the beginning of extragalactic research in the 1920s galaxies were thought to be in general 'islands', i.e. isolated stellar systems, with just a few obvious exceptions like the M51 system. The success of the Hubble classification could have been a reason to discard systems not fitting into it. Thus less regular systems have been neglected – by definition – as peculiar. The interest in these systems raised strongly when new catalogues by Vorontsov-Velyaminov (1959) and Arp (1966) became available. They demonstrated that even the peculiar objects have a lot of common features like bridges, tails, or rings. Additionally, better observational instruments allowing for deeper

images and new wavelength ranges revealed more complex structures. Thus, a lot of galaxies formerly classified as non-interacting may have had some gravitational interaction in the past which is still reflected in e.g. warps, flares, or thick discs. Especially useful are HI observations which can cover a much larger radial extension than the optical images. Therefore, HI is a very good tracer for tidal interactions.

The theoretical understanding of interacting galaxies suffered for a long time from the lack of computational power allowing for a numerical solution of the gravitational N-body problem. After a remarkable treatment by Holmberg (1941) who built an analogue computer (consisting of light bulbs and photo cells) for determining the gravitational force, it took 20 years until N-body simulations were performed on a general purpose computer (Pfleiderer & Siedentopf, 1961): The basic idea of these *restricted N-body* simulations was the assumption that the potential in interacting galaxies can adequately be modeled by two particles which represent the galactic masses and move under their mutual gravitation, i.e. on Keplerian orbits. With these assumptions all the other particles are just test particles, and the complete N-body problem has been reduced to  $N$  single body problems for a time-dependent potential. In a remarkable series of simulations Toomre & Toomre (1972) applied this technique in order to determine the parameters of a couple of well studied interacting systems like Arp 295, M51 + NGC5195, or NGC4038/39. Motivated by these simulations and by a remarkable coincidence of the estimated fraction of strong interactions with the fraction of elliptical and S0 galaxies Toomre (1977) put forward the idea of a merger origin of elliptical galaxies. Hence, a whole class of galaxies would have been formed mainly by strong interactions. However, restricted N-body simulations were not able to check this idea, because they do not include processes like dynamical friction or transfer of orbital angular momentum of the galaxies into galactic spin in a self-consistent manner. Moreover, the assumption of unaffected point-like galaxies becomes rather poor for merging systems. Thus, computationally much more expensive self-consistent calculations were required. Already first models using  $N = 500$  particles proved the idea of merging (White, 1978; Gerhard, 1981).

With increasing computational power new N-body techniques have been developed which increased the accessible particle number by many orders of magnitude. Especially the TREE-method developed by Barnes & Hut (1986) and Hernquist (1987, 1990) was perfectly suited for interacting systems, because the organization of the force calculation – the most time consuming part of N-body calculations – adapts in the TREE scheme easily and automatically to clumpy mass distributions for a moderate computational price ( $\sim O(N \log(N))$ ) compared to direct simulations ( $\sim O(N^2)$ ). By this, Barnes (1988) was able to simulate encounters of disc galaxies including all dynamical components, i.e. the disc, the bulge, and the halo as N-body systems. Compared to faster grid-based methods (e.g. Sellwood, 1980) or expansion methods (e.g. Hernquist & Ostriker, 1992) direct N-body simulations (or semi-direct methods like TREES) seem to be more flexible with respect to strongly varying geometries and scalelengths. An alternative to these sophisticated numerical techniques is the use of special purpose computers like the machines of the GRAPE project (Sugimoto et al., 1990). They implement Newton’s law of gravity (modified for gravitational softening) in the hardware which allows for a very fast direct determination of the gravitational forces, though there still exists the

$N^2$  bottleneck. E.g. for simulations with  $N = 10^5$  particles a GRAPE3af (with 8 GRAPE processors) is competitive with a TREE-code running on a CRAY T90.

Simultaneous to the development of efficient stellar N-body integrators mainly two methods (based on particles) for the treatment of a dissipative, star-forming gas component have been applied: The *smoothed particle hydrodynamics* scheme (SPH) solves the gasdynamical equations, i.e. the diffuse nature of the interstellar medium (ISM) is emphasized (e.g. Hernquist & Katz, 1989). An alternative approach focussed on the clumpiness of the clouds in the ISM. These clouds were treated as *sticky particles*: Without physical collisions with other clouds or close encounters they move on ballistic orbits like stars. However, in case of a collision the clouds might merge or loose kinetic energy depending on the adopted microphysics (e.g. Casoli & Combes, 1982; Palouš et al., 1993; Theis & Hensler, 1993).

By these technical and numerical improvements of the last 10 years reliable N-body simulations even for the infall of small satellites into larger galaxies have become possible (e.g. Quinn et al., 1993; Walker et al., 1996; Huang & Carlberg, 1997; Velázquez & White, 1998). The interest in these minor mergers raised especially after the discovery of the Sagittarius dwarf galaxy SgrI which seems to be an ongoing merger with the Milky Way (Ibata et al., 1994), i.e. minor mergers seem to be a common phenomenon. This is in agreement with estimates based on the cosmological CDM model which predicts that 85% of the finally existing galaxies have undergone a merger with a companion of at least 20% of its own mass (Frenk et al., 1988). Despite some debate on this high merging rate (Tóth & Ostriker, 1992) tidal interaction or at least minor merging seem to be a normal evolutionary process for a large fraction of giant galaxies.

Though there is a large number of papers dealing with principle effects of interactions like tidal tails or induced star formation, there exist considerably fewer papers about the modeling of special objects (e.g. Salo & Laurikainen (1993) on NGC7752/53 or Thomasson & Donner (1993) on M81 and NGC3077). This deficiency is mainly caused by two reasons: First, for a detailed confrontation of theory with observation high resolution data in configuration and velocity space are required. These should cover a large fraction of the space between the interacting galaxies. In principle, HI would be a good tracer for the global dynamics, however, there are just a few observational sites which give data of sufficient quality.

The second problem is the large parameter space resulting in two connected difficulties: finding a good fit at all and determining its uniqueness (or other acceptable parameter sets). Observationally only three kinematical quantities – the projected position on the sky and the line-of-sight velocity – can be measured. So, for each galaxy the line-of-sight position and the two components of the velocity in the plane of the sky are unknown. Another parameter, the galactic mass, depends on the availability of velocity data, the determination of the distance, and the reliability of the conversion from velocity to masses. These 14 parameters just fix the orbit in case of a two-body interaction. Moreover, one has to specify the parameters that characterize both stellar systems, e.g. characteristic scales, orientation, or rotation of a disc. By this one ends up with a high-dimensional parameter space which is – even including some 'prejudices' about the system – in general too large for a standard search method. For instance, let us assume that the orientation, rotation, and scale length of the discs, the galactic masses and all the 6 available

kinematic data are known. The remaining parameter space has still 6 dimensions. A regular grid with a poor coverage of 10 grid points per dimension demands  $10^6$  models or 340 years GRAPE simulation time (assuming 3 CPU-hours for a complete calculation) or still a month with a restricted N-body program (assuming 3 CPU-seconds per simulation).

An alternative approach to investigate large parameter spaces are genetic algorithms (Holland, 1975; Goldberg, 1989). The basic idea is to apply an evolutionary mechanism including 'sexual' reproduction operating on a set of parameters which are selected for parenthood according to their 'fitness'. The fitness is determined by the ability of the parameters to reproduce the observations, whereas the reproduction is done by 'cross-over' of the parental parameters and applying a 'mutation' operator. Though genetic algorithms (GA) have been used in many branches of science, there are just a few applications in astrophysics, e.g. for fitting rotation curves or analysis of Doppler velocities in  $\delta$  Scuti stars (for a review see Charbonneau, 1995). Recently, Wahde (1998) demonstrated the ability of genetic algorithms to recover orbital parameters for artificial data generated by N-body simulations of strongly interacting galaxies. He stressed that in these systems the positional information can be already sufficient to determine the orbital elements.

In this paper I want to demonstrate how different N-body techniques can be combined in order to create a model for the dynamics of interacting galaxies provided the intensity distribution is available. The scheme consists basically of two steps. In the first step restricted N-body simulations will be performed to constrain the model parameters: If a sufficient accurate data set is available, the genetic algorithm will be used to find the orbital parameters and to check the uniqueness of the result. Additionally, the sensitivity of the solution can be checked by an extended parameter study. Alternatively, in case of insufficient data, one could at least use the restricted N-body models to get a first guess of the parameters, by this creating an artificial intensity map and then applying the genetic algorithm to check its uniqueness. In the second step self-consistent models are necessary in order to 'tune' the parameters and to check the applicability of the restricted N-body method. These checks have to address two questions: Is the neglect of self-gravity acceptable? Does gas dynamics alter the results significantly? Technically this means that self-consistent simulations with and without gas have to be performed.

The numerical models of this paper are performed with respect to NGC4449 which is a prototype of an actively star-forming galaxy similar in size and mass to the Large Magellanic Cloud. NGC4449 is surrounded by an extended HI halo which shows some distortion (van Woerden et al., 1975; Bajaja et al., 1994). Hunter et al. (1998) published recently high resolution HI images taken at the VLA showing a large scale lopsided structure. Though there seems to be a close dwarf companion, DDO 125, it is not clear whether the observed streamers are tidal tails caused by an interaction with DDO125 (Hunter et al., 1998). For example, tidal distortions are missing in the optical image of both galaxies and no clear bridge has been detected. However, assuming a face-on encounter Theis & Kohle (1998) demonstrated qualitatively by N-body simulations that the main HI-features could stem from such an encounter provided the mass of DDO125 exceeds 10% of the mass of NGC4449. An alternative scenario assumes that the HI structure is an

ongoing infall of gas onto NGC4449. This might be caused by the encounter with DDO125 followed by a compression and cooling of the gas resulting in an infall of the gas (Silk et al., 1987). However, it seems to be difficult that the observed large-scale, lopsided and regular structure in NGC4449 can be maintained over a typical timescale like the orbital period which is longer than 1 Gyr for the outer streamer. Already the high internal velocity dispersion of  $10 \text{ km s}^{-1}$  would destroy the streamers on a timescale of  $2 \cdot 10^8 \text{ yr}$  (Hunter et al., 1998). In this paper I investigate the interaction scenario addressing the question whether the observed structures can be formed by tidal interaction at all and what the constraints on the mass distribution or the orbits of both galaxies are.

Sect. 2 summarizes the observational data of NGC4449 and DDO125 relevant for the models of this paper. The different modeling techniques and the numerical results are described in Sect. 3: First, the restricted N-body method is introduced (Sect. 3.1) and a set of first results is shown in Sect. 3.2 and 3.3. Afterwards the genetic algorithm approach is explained in Sect. 3.4 and its results are shown in Sect. 3.5. Finally, the restricted N-body simulations are compared with self-consistent models with (Sect. 3.7) and without gas (Sect. 3.6). The results of these different approaches are summarized and discussed in Sect. 4.

## 2 The case of NGC4449 and DDO125

### 2.1 NGC4449

When the optical images of NGC4449 and the Large Magellanic Cloud are compared, many similarities like the presence of a bar, the size or the total luminosity are found. However, different to the LMC, which has the Milky Way in its neighbourhood, NGC4449 seems to be a perfect candidate to study the properties of a genuine Magellanic type irregular unaffected by the tidal field of a large galaxy. Its distance of  $2.9 - 5.6 \text{ Mpc}^1$  allows also for detailed investigations which were performed in the visual (e.g. Crillon & Monnet, 1969; Hunter & Gallagher, 1997), in the radio band (e.g. van Woerden et al., 1975; Klein et al., 1996), in the HI emission line (e.g. Bajaja et al., 1994; Hunter & Gallagher, 1997; Hunter et al., 1998), in the CO emission line (e.g. Sasaki et al., 1990; Hunter & Thronson, 1996; Kohle et al., 1998), in the infrared (e.g. Hunter et al., 1986), in the FUV (e.g. Hill et al., 1994) and in X-rays (e.g. della Ceca et al., 1997; Bomans & Chu, 1997). Inside the Holmberg diameter of 11 kpc NGC4449 shows ongoing strong star formation along a bar-like structure (Hill et al., 1994). This activity seems to induce a variety of morphological features like filaments, arcs, or loops which have a size of several kpc (Hunter & Gallagher, 1997).

Already the early radio observations of van Woerden et al. (1975) exhibited a large HI-structure exceeding the Holmberg diameter of 11 kpc by a factor of 7.5. Recent observations by Bajaja et al. (1994) with the Effelsberg telescope and

---

<sup>1</sup>Most of the distance estimates of NGC4449 differ mainly because of the assumed value  $H_0$  for the Hubble constant. Independently of  $H_0$  Karachentsev & Drozdovsky (1998) derived from the photometry of the brightest blue stars a distance of 2.9 Mpc. However, the error of this measurement is unclear. In accordance with Hunter et al. (1998) a distance of 3.9 Mpc will be assumed in this paper. Thus,  $1'$  corresponds to 1.1 kpc.

Figure 1: *Contour map of the integrated HI-image of NGC4449. NGC4449 is at the center of the image and DDO125 is located at the almost circular contours in the South. This image was kindly provided by Deidre Hunter.*

more detailed results by Hunter et al. (1998) with the VLA revealed a complex structure of several components (Fig. 1): An elongated ellipse of HI gas centered on NGC4449 has a total mass of  $\sim 1.1 \cdot 10^9 M_{\odot}$ . This gas rotates rigidly inside 11 kpc reaching a level of  $97 \text{ km s}^{-1}$  in the deprojected velocity. Outside 11 kpc the rotation curve is flat. Bajaja et al. (1994) derived a dynamical mass of  $7.0 \cdot 10^{10} M_{\odot}$  inside 32 kpc and a HI gas mass fraction of 3.3%. Within 11 kpc the dynamical mass is  $2.3 \cdot 10^{10} M_{\odot}$  and the mass inside the optical radius of about 5.6 kpc is  $3 \cdot 10^9 M_{\odot}$ . Applying single dish data for a 21' beamwidth Hunter et al. (1998) derive about  $10^{10} M_{\odot}$ . Kinematically interesting is the counterrotation of the HI gas inside the optical part of NGC4449 with respect to the outer regions. For the central ellipse Hunter et al. (1998) determined a position angle of  $230^{\circ} \pm 17^{\circ}$  and an inclination of  $60^{\circ} \pm 5^{\circ}$ .

South of the galactic center a streamlike structure of 25 kpc emanates which abruptly splits into two parts: A small spur (5 kpc) which points towards DDO125, a close irregular galaxy, and a long extended stream. The latter first points 24 kpc to the north (in the following: '*vertical streamer*'), then 49 kpc north-east and, finally, 27 kpc to the south-east (together called the '*northeastern streamer*'), by this covering  $180^{\circ}$  around NGC4449. Remarkable are the long straight sections and the abrupt changes of direction. The total mass of the streamers measured by the VLA observations is about  $1 \cdot 10^9 M_{\odot}$ . Hunter et al. (1998) pointed out that by comparison with Effelsberg data there is an additional diffuse HI mass not detected in the VLA observations which amounts to two-thirds of the HI in the extended structures.

## 2.2 DDO125

DDO125 is located in the south-east of NGC4449 at a projected distance of 41 kpc. The line-of-sight velocity difference between DDO125 and NGC4449 is only about  $10 \text{ km s}^{-1}$ . Tully et al. (1978) found rigid rotation inside the optical radius of DDO125 and an inclination of the adopted disc of  $50^{\circ}$ . From this they derived a total mass of  $5 \cdot 10^8 M_{\odot}$  (corrected for a distance of 3.9 Mpc) which is in agreement with single dish observations (21' beamwidth) of Fisher & Tully (1981). However, Ebnetter et al. (1987) reported VLA-observations which show a linear increase of the rotation curve out to the largest radii where HI has been detected, i.e. out to twice the optical radius. This already allows for an estimate of a lower mass limit for DDO125 which is a factor 8 larger than the value of Tully et al. (1978), i.e.  $4 \cdot 10^9 M_{\odot}$ . Since neither flattening of the rotation curve nor any decline has been observed, this value is only a lower limit. If one compares that mass with the *total* mass of NGC4449 derived by Bajaja et al. (1994) one gets a mass ratio of about  $q \approx 5.7\%$  which is, however, just a lower limit. Comparing the masses inside the fiducial range of rigid rotation gives a higher mass ratio of  $q \approx 17.4\%$ .

### 3 Numerical Modeling

For the simulations described in this paper three different N-body approaches have been applied: The method of restricted N-body simulations (Pfleiderer & Siedentopf, 1961; Toomre & Toomre, 1972) is described in Sect. 3.1. The self-gravitating models are split into calculations without gas (Sect. 3.6) and simulations which include gas by means of sticky particles (Sect. 3.7).

The advantage of the first method is the reduction of the full N-body problem to  $N$  single body problems and the use of particles as 'test particles' which gives high spatial resolution at the places of interest for almost no computational cost. Furthermore, the CPU-time scales linearly with particle number which is superior to almost all N-body codes. Because of this the calculation is 1000 times faster than self-consistent simulations. Hence, the restricted N-body calculation is at the moment the only method which allows about  $10^4$  simulations in a couple of CPU-hours. Such a fast computation is a prerequisite for all systematic searches in parameter space like the genetic algorithm described in Sect. 3.4.

On the other hand, the simplified treatment of the galactic potential in restricted N-body simulations prohibits any effect of the tidal interaction on the orbits of both galaxies, e.g. no transfer of orbital angular momentum into galactic spin is possible (i.e. no merging). In order to overcome this problem, the results of restricted N-body models and genetic algorithms must be compared with detailed self-consistent simulations. In a first step the stellar dynamical applicability of the restricted models is checked by a comparison with self-gravitating systems calculated with a GRAPE3af special purpose computer (Sugimoto et al. 1990; see Sect. 3.6).

So far the dynamics of the system has been investigated in terms of stellar dynamics, though in many cases (and also in the case of NGC4449) HI *gas* is observed. In general, the effects of neglecting gasdynamics are not clear. E.g. a purely stellar dynamical ansatz was successfully applied for the system M81 and NGC3077 (Thomasson & Donner, 1993), whereas in other systems the dynamics of the gas can deviate strongly from the behaviour of the stars (e.g. Noguchi, 1988; Barnes & Hernquist, 1996). Therefore, one has to compare stellar and gas dynamical results which is done in this paper by a sticky particle method (Sect. 3.7).

The units are chosen to 1 kpc,  $7 \cdot 10^{10} M_{\odot}$  (the fiducial mass of NGC4449) and  $G=1$ , which result in a time unit of 1.78 Myr and a velocity unit of 549 km s<sup>-1</sup>.

#### 3.1 Restricted N-body models

The basic idea of restricted N-body simulations is to reduce the N-body problem to  $N$  1-body problems by assuming that the gravitational potential is given by a simple relation, e.g. a two- or a few-body problem which has a known (semi-) analytical solution or can be solved by fast standard methods. Here I assume that the gravitational forces on each particle are given by the superposition of the forces exerted by two point-like objects (the galaxies) moving on Keplerian orbits. Thus, for the orbits one has to specify 12 parameters which reduce to 6 in the center-of-mass frame: The orbital plane is fixed by the inclination angle

and the argument of the ascending node. The orbit itself is characterized by its eccentricity and the location of the pericenter, i.e. the pericentric distance and the argument of the pericenter. Finally, the initial location of the 'reduced' particle (or the time of pericentric passage) has to be specified to fix the phase. For a comparison with the observations the masses of the galaxies and the phase of the observation have to be supplied, too. Three of the six orbital parameters can be fixed by the observed location of both galaxies on the plane of sky ( $x$ - $y$  plane) and the line-of-sight velocity. The masses can be estimated by the velocity profiles of the galaxies provided the distance to them is known.

In this paper the time of pericentric passage is set to zero. As input the orbital eccentricity and inclination and the minimum distance are given. Furthermore, the directly observable parameters, i.e. the masses of the galaxies, the projection of the relative position of both galaxies on the plane of sky, and their line-of-sight velocity difference are supplied. They are used to determine the argument of the pericenter, the phase (or time since pericentric passage) of the observed system and the argument of the ascending node of the orbital plane. Additionally, the initial distance or phase has to be specified: In case of parabolic and hyperbolic encounters the distance was set to 100 kpc, which guarantees a sufficient low tidal influence at the start of the simulation. In case of an elliptical encounter, the situation is more difficult, because the apocentric distance might be small, especially if the eccentricity is low. Thus, the system might be affected permanently by tidal forces or even a series of repeated encounters which make the usage of the restricted N-body method doubtful. For these elliptical orbits the initial azimuthal angle of the orbit was set to  $120^\circ$  ( $0^\circ$  corresponds to pericenter).

The test particles are arranged in a flat disc moving on circular orbits. The disc itself is characterized by its orientation, i.e. its inclination and position angle, the scalelength and the outer edge. Additionally, an inner edge can be specified in order to avoid a waste of computational time by integrating tidally unaffected orbits well inside the tidal radius of the galaxy. In most of the restricted N-body simulations the test particles are distributed in 30 to 60 equidistant rings of 125 particles, i.e. a total of  $N = 3750$  to 7500 particles. The typical spacing of the rings is 0.7 to 1.5 kpc depending on the outer edge of the disc. The time integration of the equations of motion is performed by a Cash–Karp Runge–Kutta integrator of fifth order with adaptive timestep control (Press et al., 1992). In order to prevent a vanishingly small timestep by an accidental infall of a test particle to the galactic center, the gravitational force is softened on a length scale of 1 kpc. In order to speed-up the calculation the galactic positions are tabulated by cubic splines and the integrator uses these look-up tables. On a SPARC10 with a 150 MHz CPU a typical 7500-particle encounter takes 23 CPU seconds, which can be reduced by a factor of 2-3 by applying an inner edge of 10 kpc. For a typical genetic algorithm simulation with 900 particles and no offset for an inner edge 2 CPU seconds are required per simulation.

### 3.2 A first guess

In a series of simulations the orbital parameters (minimum distance  $d_{\min}$ , the eccentricity  $\epsilon$ , the mass ratio  $q$  and the orientation of orbital plane) as well as the



Figure 2: *Temporal evolution of the particle positions projected onto the plane-of-sky for different times. Closest approach is at  $t = 0$ . The final diagram corresponds to a projected distance of 41 kpc. The mass ratio of both galaxies is set to  $q = 0.2$ . The original HI-disc has an inclination of  $i = 60^\circ$ , a position angle  $\alpha = 230^\circ$  and a radial extent of  $R_{\max} = 40$  kpc. The particles inside a radius of 10 kpc are omitted. The contour lines in the lower right diagram show the normalized surface density distribution corresponding to the particle distribution in the lower left diagram. One time unit corresponds to 1.78 Myr.*

disc parameters (size  $R_{\max}$  of the disc, its position angle  $\alpha$  and inclination  $i$ ) are varied (see Table 3.3).

The temporal evolution of the primary galaxy (NGC4449) in the reference model A is displayed in Fig. 2. At the beginning both galaxies have a distance of 100 kpc corresponding to 995 Myr before closest approach. The particles inside 10 kpc are omitted for an easier identification of the evolving structure. This neglect does not alter the results, since the related particles are only weakly affected by the interaction, as the persistence of the elliptical shape of the 'central hole' demonstrates. At the moment of closest approach ( $t = 0$ ), only the outer region of NGC4449's disc reacted on the intruder. 71 Myr later (i.e. system time 40), a dense outer rim starting at the projected position of DDO125 and pointing to the north begins to form. Secondly, a weak bridge-like feature seems to connect both galaxies. Both features are more pronounced after 178 Myr. At that time an additional tidal feature commences to evolve north of the center. When DDO125 has a projected distance of 41 kpc which occurs 362 Myr after closest approach, three features are discernible: The remnant of the former 'bridge' starts south of the center of NGC4449 pointing to the south-west. The 'vertical feature' starts at the end of the first structure and points to the north. The third structure is a long tidal arm which starts west of NGC4449 pointing to the north-east before turning again back to the south-east.

A comparison of the intensity map of model A (lower right diagram in Fig. 2) with the observations (Fig. 1) demonstrates that the main observational features can be reproduced qualitatively by the reference model A, i.e. a parabolic orbit, a mass ratio  $q = 0.2$  and a minimum distance  $d_{\min} = 25$  kpc. The parameters for the disc orientation are chosen in agreement with Hunter et al.'s suggestion of  $i = 60^\circ$ ,  $\alpha = 230^\circ$ , whereas the disc radius was set to  $R_{\max} = 40$  kpc. Though this numerical model is not a detailed fit of the data, the characteristic sizes and locations of the streamers as well as the unaffected disc can be found. The material located between the streamer and the disc, which is not seen in Hunter's data, could correspond to the extended HI-mass detected in the single dish observations by van Woerden et al. (1975). In the following sections I will discuss the influence of the individual parameters. The global uniqueness of the reference model is investigated in Sect. 3.5.

Figure 3: *Dependence on the eccentricity. Projection of the particle positions onto the plane-of-sky in the moment of a projected distance of 41 kpc. The eccentricities of the models are 0.5 (upper left, model B1), 0.8 (upper right, B2), 1.0 (A, reference model), 1.5 (B3) and 5.0 (B4).*

Figure 4: *Dependence on the mass ratio. Projection of the particle positions onto the plane-of-sky in the moment of a projected distance of 41 kpc. The mass ratios are - starting with the upper left diagram - 0.01 (model C1), 0.05 (C2), 0.1 (C3), 0.2 (A, reference model), 0.3 (C4) and 0.4 (C5).*

### 3.3 Parameter study

In this section the influence of the basic parameters, i.e. the orientation of the orbital plane, the orbital eccentricity and the minimum distance, the mass ratio of both galaxies, the orientation of the HI disc and its extent are discussed (s. Table 3.3). In the following simulations all parameters except the one of interest are kept constant with respect to model A. Thus, the vicinity of the reference model in parameter space is studied.

**Eccentricity.** The eccentricity mainly influences the interaction timescale which is defined here as the time between maximum approach and a projected distance of 41 kpc, i.e. the moment of observation. An eccentricity of 5.0 (corresponding to a hyperbolic encounter) decreases the interaction time by a factor 2.6 resulting in less 'damage' of the primary galaxy (Fig. 3): Only the remnant of the 'bridge' feature can be discerned, whereas the other two streamers found in the reference model are missing completely. With decreasing eccentricity the north-eastern streamer becomes pronounced before the vertical structure arises. The latter is weakly expressed for  $\epsilon = 1.5$ . Reducing  $\epsilon$  further to bound orbits makes the features even more prominent. In case of  $\epsilon = 0.5$  the north-eastern and the vertical streamer form even a single structure clearly detached from the center. However, due to the strength of the interaction a second broad tidal 'arm' is ejected from NGC4449 leaving a low-density region south to the northern tip of the north-eastern streamer.

**Mass ratio.** The variation of the mass ratio gives a lower limit of about 10% in order to create a sufficient tidal response (Fig. 4). If the mass ratio exceeds 0.3, the 'vertical feature' becomes less vertical and the north-eastern streamer is more diffuse, both due to the enhanced tidal pull by the intruder.

**Minimum distance.** Though the interaction time is not strongly influenced by the minimum distance  $d_{\min}$ , it determines the maximum strength of the tidal field (Fig. 5): For small separations the structures become more diffuse and the primary is much stronger affected. The vertical feature is much more extended creating an additional tidal 'arm' (similar to the model with an orbital eccentricity  $\epsilon = 0.5$ ). If the distance of closest approach exceeds 30 kpc, almost no streamers are formed.

**Orbital plane.** The orientation of the orbital plane characterizes basically the

*Model parameters of the restricted N-body simulations*

model	$\epsilon$	$q$	$d_{\min}$	$i$	$i_d$	$\alpha_d$	$R_{\max}$	comment
A	1.0	0.2	25	40	60	230	40	reference model
B1	0.5	0.2	25	40	60	230	40	eccentricity
B2	0.8	0.2	25	40	60	230	40	
B3	1.5	0.2	25	40	60	230	40	
B4	5.0	0.2	25	40	60	230	40	
C1	1.0	0.01	25	40	60	230	40	mass ratio
C2	1.0	0.05	25	40	60	230	40	
C3	1.0	0.1	25	40	60	230	40	
C4	1.0	0.3	25	40	60	230	40	
C5	1.0	0.4	25	40	60	230	40	
D1	1.0	0.2	15	40	60	230	40	minimum distance
D2	1.0	0.2	20	40	60	230	40	
D3	1.0	0.2	30	40	60	230	40	
D4	1.0	0.2	35	40	60	230	40	
D5	1.0	0.2	40	40	60	230	40	
E1	1.0	0.2	25	10	60	230	40	orbital inclination
E2	1.0	0.2	25	20	60	230	40	
E3	1.0	0.2	25	30	60	230	40	
E4	1.0	0.2	25	50	60	230	40	
E5	1.0	0.2	25	70	60	230	40	
F1	1.0	0.2	25	40	40	230	40	disc inclination
F2	1.0	0.2	25	40	50	230	40	
F3	1.0	0.2	25	40	70	230	40	
G1	1.0	0.2	25	40	60	210	40	pos. angle of disc
G2	1.0	0.2	25	40	60	250	40	
H1	1.0	0.2	25	40	60	230	25	outer edge of disc
H2	1.0	0.2	25	40	60	230	30	
H3	1.0	0.2	25	40	60	230	35	
H4	1.0	0.2	25	40	60	230	50	

Table 1: *Parameters of the different restricted N-body models: model name (col. 1), orbital eccentricity  $\epsilon$  (col. 2), mass ratio  $q$  of both galaxies (col. 3), minimum separation  $d_{\min}$  of galactic centers (in kpc, col. 4), inclination  $i$  of orbital plane (in degrees, col. 5), orientation of NGC4449 disc (in degrees): inclination  $i_d$  (col. 6) and position angle  $\alpha_d$  (col. 7), maximum radius  $R_{\max}$  of gaseous disc (in kpc, col. 8).*

Figure 5: *Dependence on the minimum distance during the encounter. Projection of the particle positions onto the plane-of-sky in the moment of a projected distance of 41 kpc. The minimum distances are - starting with the upper left diagram - 15 kpc (model D1), 20 kpc (D2), 25 kpc (A, reference model), 30 kpc (D3), 35 kpc (D4) and 40 kpc (D5).*

Figure 6: *Dependence on the inclination angle of the orbital plane. Projection of the particle positions onto the plane-of-sky in the moment of a projected distance of 41 kpc. The inclinations are  $10^\circ$  (upper left, model E1),  $20^\circ$  (upper right, E2),  $30^\circ$  (E3),  $40^\circ$  (A, reference model),  $50^\circ$  (E4) and  $70^\circ$  (E5).*

Figure 7: *Dependence on the extension of the HI distribution in NGC4449. Projection of the particle positions onto the plane-of-sky in the moment of a projected distance of 41 kpc. The radial extensions are 25 kpc (upper left, model H1), 30 kpc (upper right, H2), 35 kpc (H3), 40 kpc (A, reference model) and 50 kpc (H4).*

observer’s location or the line-of-sight which is fixed by two parameters. For the models here only the orbital inclination is a free parameter, since the second parameter, the position angle of the orbital plane, is fixed by the observed relative line-of-sight velocity of both galaxies. The models show that the inclination mainly affects the orientation of the vertical streamer (Fig. 6): An inclination outside the range  $[30^\circ, 50^\circ]$  gives too much deviation from the south-north direction of the vertical feature.

**HI distribution in NGC4449.** A specification of the mass- and especially the HI-distribution is a more difficult task, because contrary to the well-known two-body problem the number of free parameters characterizing the structure and internal dynamics of the interacting galaxies is unknown and a matter of investigation itself. For example, it is not a priori clear whether the HI is distributed like a disc, a spheroid, or something else. In order to reduce the number of free parameters I will assume here that the observed inner elongated ellipse is the remnant of an original exponential HI disc, which can be specified by its orientation (which is observed!), its scale length and radial extent. Since the particles are treated as test particles, a variation of the scale length does not change the final location of a particle, but its mass which is required for the calculation of the intensity map. A small scale length (e.g. 5 kpc) would confine too much HI in the center that is unaffected by the encounter. Since the observations show that a large fraction of HI is outside 20 kpc, I have chosen a large scale length of 30 kpc which gives only a weak radial decline of the HI surface density and, by this, a sufficient amount of HI in the outer regions.

DISC SIZE. The influence of the maximum radius  $R_{\max}$  of the disc is shown in Fig. 7. If  $R_{\max}$  is smaller than 35 kpc, the vertical streamer has not been formed at all indicating that this feature stems from the HI gas far outside the center. The

Figure 8: *Dependence on the orientation of the HI disc in NGC4449. Projection of the particle positions onto the plane-of-sky in the moment of a projected distance of 41 kpc. The orientation is characterized by the inclination  $i_d$  of the disc and the position angle  $\alpha_d$ :  $i_d = 60^\circ, \alpha_d = 230^\circ$  (upper left, model A, reference model);  $60^\circ, 210^\circ$  (upper right, G1);  $60^\circ, 250^\circ$  (G2);  $40^\circ, 230^\circ$  (F1);  $50^\circ, 230^\circ$  (F2) and  $70^\circ, 230^\circ$  (F3).*

north-eastern arm and the 'bridge', however, are already built up for  $R_{\max} = 25$  kpc. With increasing disc size the vertical streamer becomes more pronounced and longer which excludes disc sizes larger than 45 kpc.

DISC ORIENTATION. The orientation of the HI disc also strongly affects the appearance of the primary galaxy. A variation of the position angle  $\alpha$  by  $20^\circ$  gives already HI distributions which are incompatible with the observations (Fig. 8). If  $\alpha$  is decreased, the vertical streamer is more extended and diffuse. On the other hand, if  $\alpha$  is increased, the north-eastern arm becomes too long and the vertical feature vanishes almost completely. Similarly, the results depend strongly on the inclination  $i$ : Inclinations below  $50^\circ$  give only weak bridges and weak vertical streamers, whereas the orientation of the 'vertical' streamers deviates strongly from the northern direction for inclinations exceeding  $70^\circ$ .

The performed parameter study demonstrates that even close to the parameters of model A, the final particle distribution shows significant variations which are not in agreement with the observations. Thus, the reference model might be a good and locally unique candidate describing the dynamics of NGC4449 and DDO125. The confidence in this encounter scenario is especially enhanced by the strong dependence on the orientation of the HI disc of NGC4449. Qualitatively good models are only found, if the disc orientation agrees with the values determined independently by observations. On the other hand, the former parameter study only investigates a small fraction of parameter space and, thus, the uniqueness of the solution is not confirmed. Moreover, in general it is very tedious to find a good model 'by hand', i.e. by an unsystematic non-automated search in parameter space. Thus, the probability to accept the first solution found seems to be very large (especially, if CPU intensive simulations are performed), by this neglecting other regions in parameter space which might also give acceptable fits. In the next section an automatic search in parameter space by means of a genetic algorithm is introduced. This allows in principle for an *ab initio* determination of acceptable parameter sets (if data sets of sufficient quality are available) or at least for a uniqueness test of a favoured scenario like the reference model described above.

### 3.4 A systematic search using a genetic algorithm

The idea of applying models of organic evolution for optimization problems in engineering dates back to the 1960s and 1970s (e.g. Rechenberg, 1965; Schwefel, 1977). Different to standard gradient techniques for optimization which work deterministically (e.g. the downhill simplex method (Press et al., 1992)) Rechenberg's concept of '*Evolutionstrategie*' is a probabilistic one: Starting with a more or less random individual ('*parent*'), i.e. a single point in search space, a '*child*' is generated by a random mutation of the parameter set characterizing the parent. The quality of both individuals with respect to the optimization problem (i.e. their '*fitness*') determines now the parent of the next generation. Repeating this process of mutation and selection improves the quality of the individual monotonously. This simple evolutionary strategy, which is just a special implementation of evolutionary algorithms (EAs) in general, demonstrates the advantages of these methods: Compared to complete grids in the parameter space the probabilistic, but oriented nature of

Figure 9: *Fitness and best fit of an early generation during the GA fitting procedure. The figure displays the artificial original data (left column: positions of the particles in the x-y-plane (upper left) and the resulting intensity contour lines (linear spacing, lower left), the best fit of the actual generation (middle column) and information about the fitness history, i.e. the maximum fitness (upper right) and the actual fitness distribution (lower right). The underlying grid in the left and middle column is used to determine the intensities.*

the evolutionary search strategy allows for an efficient check of a high-dimensional parameter space. Compared to gradient methods which are very fast near the optimum, EAs do not need any gradient information which might be computationally expensive. Additionally, they depend only weakly on the starting point and - most important - they are able to leave local optima. The price for these features is a large number of fitness evaluations or test points in search space before converging to a good solution.

Holland (1975) extended the *Evolutionstrategie* of Rechenberg by abandoning asexual reproduction: He used a population of individuals instead of a single individual (and its offsprings). From the population two individuals were selected according to their fitness to become parents. These parents represent two points ('chromosomes') in search space and the corresponding coordinates are treated like genes on a chromosome. These chromosomes are subject to a *cross-over* and a *mutation* operator resulting in a new individual which is a member of the next generation. This breeding is repeated until the next generation has been formed. Finally, the whole process of sexual reproduction is repeated iteratively until the individuals representing a set of points in parameter space confine sufficiently one or several regions of high fitness. Despite many differences in the detailed implementations of genetic algorithms (GAs), the basic concept of an iterated application of randomized processes like recombination, mutation, and selection on a population of individuals remains in all GAs (Goldberg, 1989; Bäck, 1996).

For the optimization problem of fitting an N-body simulation to a given observation, I will briefly describe the main ingredients of my fitting GA-program in the following sections. The GA used here is a slightly modified version of P. Charbonneau's code PIKAIA (for details see Charbonneau (1995)).

### 3.4.1 Fitness and parent selection

In order to determine the fitness of an individual (i.e. a special parameter set), the N-body simulation has to be performed and compared with the observation. This is done by mapping the particles on a quadratic grid of size 60 kpc centered on NGC4449. The resolution of the grid was set to 7x7 in order to allow for a better resolution of the tidal features of an encounter. For each grid cell the 'intensity' was calculated by summing up the masses of the individual particles in that cell. The conversion to observed intensities can be performed by assuming a mass-to-light ratio for the particles (or treating it as another free parameter) or by normalizing the intensities. Here the intensities are normalized to the total intensity of the whole grid. The quality can be measured now by the relative deviation  $\delta$  of the

intensities in both maps:

$$\delta \equiv \sum_{i(\text{cells})} \frac{|I_{\text{ref},i} - I_{\text{mod},i}|}{\max(I_{\text{ref},i}, I_{\text{mod},i})} \quad (1)$$

The fitness  $f$  is then estimated by

$$f \equiv \frac{1}{1 + \delta}. \quad (2)$$

In case of an impossible parameter configuration (e.g. a circular orbit with a distance less than the observed projected distance) or any convergence problems the fitness of that point in search space is set to zero prohibiting any offsprings. Typically only a few models in  $10^4$  parameter sets fail, most of them in the first few generations before the system starts to approach the search space region of interest.

In order to determine the parents of the next generation the members of the actual generation are ranked by their fitness. Then the parents are selected randomly, whereas the probability to be chosen is proportional to the rank (*'roulette-wheel selection'*).

A typical example for the status of the GA after a couple of generations is shown in Fig. 9. In the left column the positions of the original data are discretized on the grid to yield the intensities displayed on the lower left. It should be noted that the resolution of the grid is about 8.6 kpc which rather exceeds the thickness of the tidal structures. In the middle column the best fit of the actual (here 7th) generation agrees already qualitatively with the original. The quality of the fit is calculated only by a comparison of the lower two intensity diagrams. The fitness distribution in the population resembles a Gaussian at the beginning of the fitting procedure.

### 3.4.2 Coding of parameters

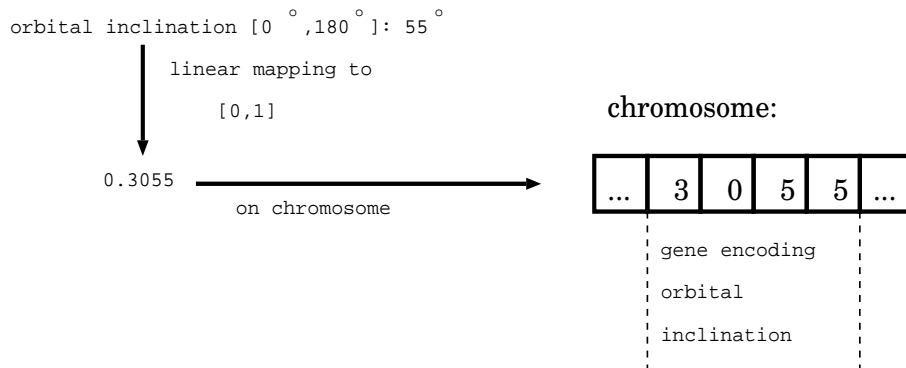


Figure 10: *Schematic diagram for the coding of parameters on a numerical chromosome.*

In organic systems the information is coded in genes in form of sequences of the four nucleotide bases where a triplet of them (a codon) encodes one amino acid, the building block of proteins. The genes themselves are arranged in one or several chromosomes which contain all the genetic information (or the genotype). The phenotype which is subject to the selection process is the result of the genetic information and the interaction with its environment.

Translated to our fitting problem, the phenotype is the final intensity map created by a special choice of parameters or initial conditions. The latter correspond to the proteins which express the genetic information physically. The mapping between the parameters and the genes or the number of chromosomes is not fixed in GAs. Many GAs apply a binary alphabet for encoding the parameters (e.g. Holland, 1975; Goldberg, 1989). In Charbonneau's program PIKAIA a decimal encoding is implemented. For my calculations I combined four decimal digits giving a number between zero and one. This 'gene' has been mapped to a real parameter by a linear or logarithmic transformation to the investigated parameter range, e.g. the orbital inclination is mapped linearly to the range  $[0^\circ, 180^\circ]$  (Fig. 10). All the genes are assumed to be located in linear manner on a single chromosome. Different to organic evolution the phenotype is completely determined by the genotype, no environmental influence on the individual is acting after its genotype is fixed.

### 3.4.3 Cross-Over

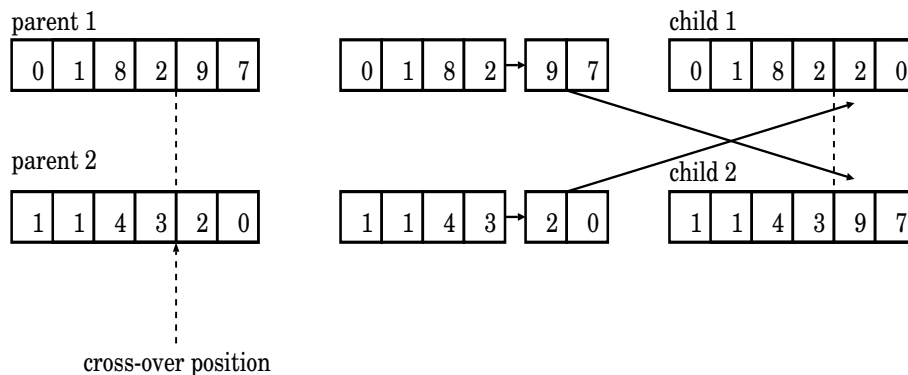


Figure 11: *Schematic diagram for the cross-over operation.*

The main difference between the evolutionary strategies and genetic algorithms is the sexual reproduction of GAs. This means that the chromosomes of the parents are combined in a new manner by means of a cross-over mechanism in addition to mutation. The principle idea is illustrated in Fig. 11: After determining the two parents a random position on the chromosomes is selected. At this position the chromosomes are split into two fragments which are exchanged among the chromosomes resulting in two new ones.



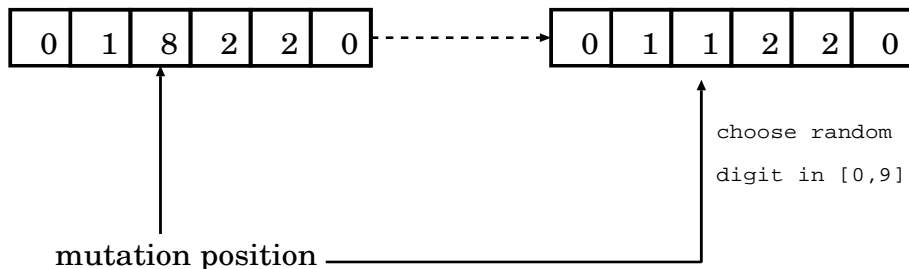


Figure 12: *Schematic diagram for the mutation process.*

### 3.4.4 Mutation

In order to introduce completely new information into a genepool a mutation process, i.e. a random change of the information in the chromosomes is introduced (Fig. 12). For each position on a chromosome mutation is applied with a small probability (typ.  $p_{\text{mut}} \approx 0.5\%$ ). After selecting a position for mutation, an integer random number in the range  $[0,9]$  replaces the original value at that position. Thus, a real change in the genetic information takes place with a probability of 90%, even if that position of a gene is subject to mutation. The overall probability for at least one 'real' mutation on a chromosome coding 6 parameters by 4 digits is about 11%. Thus, cross-over is the most important process introducing diversity into the population, whereas mutation affects only each 9th member of the population. In principle, the mutation rate can be increased, but the price would be a more or less random search in parameter space which is already after a few generations inferior to the oriented search of a GA method (Wahde, 1998).

A principle danger of GAs is inbreeding, i.e. the homogenization of the genepool by one or a few dominant genes. If they successfully replace other genes, cross-over does not introduce sufficient (or – if inbreeding is complete – any) diversity into the population and thus any further improvement of the chromosomes is prohibited. The only way to overcome this situation is to introduce more diversity by mutation. Therefore, PIKAIA allows for a variable mutation rate which increases the mutation probability  $p_{\text{mut}}$  whenever the fitness distribution becomes narrow, i.e. inbreeding is suspected to operate. On the other hand  $p_{\text{mut}}$  is decreased, if the fitness distribution becomes very broad, i.e. the randomization is supposed to be dominant.

### 3.4.5 Determination of the next generation

After  $N_{\text{pop}}$  children have been created, the old generation is completely replaced (*full generational replacement*) by the next generation. The only exception is the survival of the fittest member of the parent generation, if it is fitter than the child which would replace it (*elitism*). The latter mechanism prevents the system from forgetting successful solutions.

The initial population is randomly chosen in the accessible parameter space. A typical population size is about  $N_{\text{pop}} = 100 \dots 200$  members. The GA converges typically after about  $N_{\text{gen}} = 100$  generations. Thus,  $10^4$  or a few  $10^4$  N-body

simulations are required for a single GA fit. Self-consistent N-body models like the mentioned 3-CPU-h GRAPE models would still need 3.4 years, whereas the restricted N-body models reduce the CPU-requirement to 5.6 hours on a 150MHz-Sparc10.

### 3.5 Are the results unique?

Figure 13: *Best fit model during the course of a GA fitting procedure. The projection of the particles in x-y-plane and the corresponding grid for the intensity evaluation are displayed: The original data (upper left), the best fit of the GA after initialization (upper middle), after the first breeding (upper right), after 11 generations (lower left) and at the end of the fitting procedure after 100 generations (lower middle). The evolution of the maximum fitness is shown in the lower right diagram. The number of test particles per simulation is 900.*

In order to check the uniqueness of the reference model A, several runs with different parameter sets encoded in genes were performed. Fig. 13 shows a typical run of the GA operating on a population of 100 members. The reference model – displayed in the upper left diagram – as well as the GA models have been calculated with 900 test particles. This makes the streamers less prominent, but still discernible. The next plots show the GA status at different generations: At generation 1, the best model is just created out of the randomly chosen initial parameter sets. However, already at the second generation, i.e. the first application of the reproduction operator, the best model clearly exhibits the north-eastern streamer. At generation 11, even the weaker vertical feature and the bridge feature show up. At the end of this GA run the particle distribution of the original model A and the best fit of the GA are almost identical, at least when compared by eye. The fitness of the best fit has strongly increased from 0.04 to 0.14 where values above 0.1 indicate already a very good fit. Most of the improvements were found during the first 50 generations, i.e. analyzing 5000 models. After that generation the homogeneity of the population led to inbreeding which strongly prohibits the arise and spread of new 'better' parameters. However, this is not a problem for the models here, because a very good fit to all parameters is already found after 40 generations as the direct comparison with the parameters of the reference model demonstrates (Fig. 14). The relative deviation of the derived parameters from the original values is less than 15% in all cases, and for many of them even better than 5%.

In a series of different GA runs I varied the population size, the number of

Figure 14: *Development of six parameters of the best fit model during a GA run. The parameters are the mass of the secondary galaxy (upper left), the minimum distance (upper right), the inclination (middle left) and position angle (middle right) of the orbital plane, and the inclination (lower left) and position angle (lower right) of the disc of the primary galaxy. The filled squares show the parameters of the fitted artificial reference model.*

Figure 15: *Test of the capability of the GA (lower row) to recover original data when these data (upper row) are of low quality or incomplete. Shown are runs with low resolution, i.e. a discretization on a 4x4 grid (left column), a bad pixel (here an omitted central pixel, middle column), and a missing structure (the vertical streamer, right column).*

Figure 16: *Comparison of restricted N-body models (left) with self-consistent simulations (right) for a parabolic encounter (upper row) and an eccentricity of  $\epsilon = 0.5$  (middle row). The projected distance to the perturber is 41 kpc. The lower row displays the normalized intensity profiles for the self-consistent simulations (left:  $\epsilon = 1$ , right:  $\epsilon = 0.5$ ). Note that the surface plots are seen from north-west in order to emphasize the coherent streamer structure.*

generations or particles, the parameter combination encoded on chromosomes, the fitness function, and the random initial population. In almost all of them the best fit gave an acceptable fit of the reference model which demonstrates the capability of GAs to recover the parameters even for weak encounters. The models which failed basically suffered from inbreeding or from a fitness function which did not discriminate sufficiently between high and low quality fits. Moreover, in none of the GA runs a different region in parameter space producing a good fit ( $f > 0.1$ ) has been found. *Thus, the model A – or more exact the corresponding intensity map – seems to result from a unique parameter set.* However, this is only a 'motivated guess', not a mathematical proof!

Another interesting question is how strongly do the GA results depend on the completeness or accuracy of the data. I studied this in two ways: First, I used a coarser grid (4x4) in order to mimic a lower resolution of observational data (left column in Fig. 15). Then the GA is only qualitatively able to reproduce the reference model. Obviously, too much information is lost, when the resolution becomes too small. On the other hand, an increase of the number of cells to 10x10 did not improve the fit found on a 7x7 grid, but introduced more noise into the intensity maps. In the second test I discarded one or several grid cells from the fitness calculation (middle and right column in Fig. 15). Omitting one cell does not affect the final fit, independently of the location of the cell (here the center). However, if a whole feature like the vertical streamer is neglected, the GA is unable to recover the original data.

Figure 17: *Self-consistent N-body simulation 'sin gas': Projection of the particle positions onto the plane-of-sky at different times: initially (upper row), at closest approach (middle row) and at the projected distance of 41 kpc (lower row). The left column shows the disc particles, whereas the right column displays the halo particles.*

### 3.6 Self-consistent models 'sin gas'

The self-consistent models in this paper were performed by a direct N-body integration using the GRAPE3af board in Kiel for the calculation of the gravitational forces and potentials. The time integration was done by a leap-frog scheme with a fixed timestep of 1.78 Myr. The GRAPE board uses intrinsically a Plummer softening, the softening length was chosen to be 0.2 kpc. These choices give a total energy conservation of better than 1% during the whole simulation.

Different to the restricted N-body models the set-up of the initial particle configuration for self-gravitating systems is far from being trivial. In principle, a stable stationary stellar system fulfills the collisionless Boltzmann equation. Thus, a solution of the latter could be used as a trial galactic system. From observations of the Milky Way it is known, however, that even if the Galaxy is axisymmetric, three integrals of motion are required to construct a stationary model. Unfortunately, only two are known analytically (the energy and the  $z$ -component of the angular momentum). Additionally, even if a particle configuration is generated from a distribution function depending on the integrals of motion, it is unclear whether it is stable against perturbations which might lead to e.g. the Toomre instability or the bar instability. Thus, one has to check the stability on the timescale of interest numerically.

In this paper I use the models of Kuijken & Dubinski (1995) consisting of three components which are determined self-consistently from the Boltzmann equation: The bulge follows a King model and the halo a lowered Evans model. For the disc the third integral is approximated by the  $z$ -energy, i.e. the energy in vertical oscillations. The advantage of Kuijken & Dubinski's method is the possibility to specify parameters like scale length or scale height of the disc directly, whereas many other methods (e.g. Barnes, 1988) that start not in virial equilibrium, readjust the mass distribution on a dynamical timescale, which means less control on the structural parameters. The long-term stability has been checked by simulations of an isolated disc with  $N = 18000$  particles (8000 for the disc, 4000 for the bulge and 6000 for the halo). Within 1.5 Gyr the Lagrange radii at 10% and 90% mass vary only by 2-4%. They show no systematic trend except for a small expansion during the first 100 Myr which is probably caused by gravitational softening. Due to two-body relaxation the scale height of the disc increases by almost a factor of 2 within 1.5 Gyr. However, this heating is not expected to alter the result of the dominant interaction significantly. The Fourier amplitudes  $C_2$ , defined by  $C_m \equiv (\int_{\text{disc}} \Sigma(R, \phi) r dr e^{-im\phi} d\phi) / (\int_{\text{disc}} \Sigma(R, \phi) r dr d\phi)$  (with the surface density  $\Sigma$ ), are always less than 5%, in agreement with no significant bar or spiral pattern built up during the simulation.

Fig. 16 shows a comparison of the restricted N-body simulations with the self-consistent models. Except for the omitted central region in the former and the more diffuse structure in the latter, the large scale features are almost identical in both simulations. The differences close to the central 10 kpc (especially the phase of the 'bridge' feature in the  $\epsilon = 0.5$  model) are due to the extended dark halo in the self-consistent models. It is remarkable that the vertical and the north-eastern streamer are not affected by the halo. This confirms the applicability of the restricted N-body method here. In agreement with these simpler models the intensity maps of

Figure 18: *Projection of the particle positions onto the plane-of-sky at different times: at closest approach (upper row), at the projected distance of 41 kpc (middle row) and at the end of the simulation (lower row). Both models include self-gravity. The left column shows a purely stellar simulation, whereas the right column includes gas dynamics by means of sticky particles.*

both self-consistent models ( $\epsilon = 1.0, 0.5$ ) show clearly the streamer structure (Fig. 16).

Another interesting aspect concerns the response of the halo to the intruder. Different to the disc, the halo remains almost unchanged by the encounter (Fig. 17). This constancy of the halo potential would in principle allow to include also a rigid halo in the restricted N-body models and, hence, also in the GA fitting procedure, by this extracting information about the dark halo.

### 3.7 Self-consistent models 'con gas'

For the gasdynamical models I use a sticky particle scheme which treats each particle of the HI disc as a gaseous cloud. The radius of these clouds is assumed to follow  $R_{cl} = 20 \cdot \sqrt{M_{cl}/10^6 M_{\odot}}$  pc which is derived from the mass-radius relation of Rivolo & Solomon (1987) corrected for glancing collisions ( $M_{cl}$  is the mass of a gas cloud). When the distance of two clouds falls below the sum of their radii, merging of the clouds is allowed, if their relative orbital angular momentum is smaller than the maximum angular momentum a merged cloud can acquire before break-up. If this angular momentum criterion prevents a merger, the clouds keep their kinematical data. Star formation is only qualitatively included by adopting an upper mass limit of  $7 \cdot 10^8 M_{\odot}$  for clouds. If they exceed this limit no further merging is allowed, i.e. they are treated like stars. However, the star formation criterion is not important for the models of this paper. (For details of the cloud model or the merging mechanism see Theis & Hensler, 1993). This dissipative scheme has been successfully applied to collapsing systems reproducing many observed properties of spiral and elliptical galaxies. For the long-term evolution of barred disc galaxies a comparison of this scheme with that of Palouš et al. (1993) for  $\beta_r = \beta_t = 0.2$  gives basically the same results (Jungwiert, 1997). Thus, the chosen model should be applicable for a reliable determination of the difference between gas dynamical and purely stellar dynamical models.

A comparison of gaseous models with dissipationless models gives no significant difference (Fig. 18). Due to the low gas densities only about 20-30% of the clouds undergo inelastic collisions which are mainly occurring in the denser central regions. Thus, the outer HI halo is only very weakly influenced by (sticky particle) gas dynamics and the applicability of purely stellar simulations for the HI seems to be possible. It would be interesting to compare these models with an SPH approach emphasizing the diffuse nature of the interstellar medium.

## 4 Discussion

## 4.1 Interaction between NGC4449 and DDO125?

The previous simulations demonstrated that models based on the encounter scenario are able to reproduce the morphology of the three main streamers. Furthermore, the interaction puts gas to the south-west of NGC4449, where a clumpy HI distribution is observed (Hunter et al., 1998). Though its detailed patchy structure has not been recovered by the models, an initial gas distribution less regular than the smooth disc-like one used for the numerical models might be responsible for this deviation.

The parameter study showed that already small variations in the parameters give HI distributions which are not compatible with the observations. Especially, the strong dependence of the final structure on the initial orientation of the HI disc confines its inclination and position angle within  $10^\circ$  to the values derived *independently* from the observations. This remarkable coincidence would occur necessarily in the encounter scenario, whereas in the infall scenario it happens just by chance. A second critical feature is the abrupt direction change of the streamers. In the infall scenario they mark the path of the perturbed gas which collapses to the galactic center. However, it is hard to imagine a realistic static potential that could create orbits with such strong direction changes as e.g. from the vertical to the bridge feature. Moreover, due to the large distance of these features from the galactic center the potential should be more or less spheroidal or already spherical, which makes it even more difficult to produce such orbits.

The most critical parameter for the interaction scenario is the mass ratio  $q$  of DDO125 and NGC4449. The simulations demonstrated that a mass ratio smaller than 10% cannot reproduce the streamer structure. In order to determine  $q$ , both galactic masses have to be known. In Bajaja et al.'s (1994) estimate for the mass of NGC4449 they assumed that the HI is in rotational equilibrium even at a distance of 32 kpc. However, in case of an interaction with DDO125 the velocities at large distances might be strongly affected by the interaction and definitely not being in rotational equilibrium as the 'ejection' of the tidal arms in a continuation of the simulations demonstrates. Hence the derived mass of  $7 \cdot 10^{10} M_\odot$  is at best an upper limit to the mass of NGC4449. A better guess might be the dynamical mass inside the central gaseous ellipse which seems to be unaffected by interaction. E.g. the dynamical mass inside 11 kpc would be a factor 3 smaller than Bajaja's value. Even more difficult than for NGC4449 is the mass determination of DDO125. Observations by Tully et al. (1978) gave a dynamical mass of  $5 \cdot 10^8 M_\odot$  inside the optical radius of DDO125. However, Ebneter et al. (1987) reported a linear increase of the rotation curve exceeding the range observed by Tully et al. by a factor of two. Moreover, they found no hint for a flattening or turn-over in DDO125's rotation curve. This gives a lower mass limit of  $4 \cdot 10^9 M_\odot$ . Combining the mass estimates yield a lower limit of the mass ratio of 6% when using Bajaja's mass determination of NGC4449. A more realistic mass ratio might be derived from the ranges of rigid rotation resulting in  $q \approx 18\%$ . Thus, observationally it cannot be excluded that the mass ratio is below the critical one for the interaction scenario, however, the more realistic estimates seem to be in agreement with the values found in the simulations. The situation could be clarified when a reliable mass determination of DDO125 is available.

## 4.2 Origin of the extended HI–distribution around NGC4449

Another important question is related to the initial conditions of the previous simulations, i.e. the origin of the extended HI–distribution. In principle, there are several possibilities:

*Idea 1. The HI comes from DDO125.* In a previous encounter ( $\epsilon < 1$ ) the gas is stripped off from DDO125. Due to the long orbital period of e.g. 3.6 Gyr for  $\epsilon = 0.5$  the gas has enough time to settle down in a regular disc-like structure. However, the amount of HI gas in DDO125 is much smaller than the gas seen around NGC4449. It seems to be unlikely that DDO125 could have survived the loss of such a big fraction of its gas content without disruption.

*Idea 2. The HI comes from NGC4449.* Though a star forming dwarf galaxy drives a galactic wind e.g. by means of type II supernovae, a detailed fine–tuning of the energy injection would be required to prevent a blow–out of the HI–gas, especially if it got enough energy to form such an extended system. Moreover, the counter-rotation of the HI outside and inside the optical radius of NGC4449 makes the scenario not very appealing.

*Idea 3. The HI gas stems from a previous minor merger with NGC4449.* Though a satellite galaxy can be disrupted by the tidal field of NGC4449, it is very unlikely that it is disrupted already far outside the galactic center where the HI gas is detected.

*Idea 4. The HI originates from the collapse of a dwarf companion.* A dwarf galaxy forms in the vicinity of NGC4449. By this it undergoes a strong collapse which leads to mass ejection due to violent relaxation. In principle, a mass loss of up to 30% of the companion could occur providing enough gas to explain the HI. However, where is the dwarf today? Excluding an unlikely radial orbit, the dwarf’s orbit could in principle decay by dynamical friction. However, due to the large distance to NGC4449 the decay time should be at least several orbital periods which exceeds the Hubble time.

*Idea 5. Another major encounter.* Though NGC4449 is a member of the loose Canes Venatici group, there seem to be no close galaxy which has a radial velocity in agreement with the rotational sense of the gaseous disc in NGC4449. So, who is the partner?

## 5 Summary and conclusions

Several N-body methods are combined in order to develop a method for the determination of the parameters of interacting galaxies. This method is applied to the HI distribution of NGC4449. In a first step the fast restricted N-body method is used to confine a region in parameter space which reproduces the main observed features. In a second step a genetic algorithm (also using restricted N-body calculations) is employed which allows for both, an automatic fit of observational data even in a high-dimensional parameter space and/or a uniqueness test of a favoured parameter combination. For a genetic algorithm one typically has to follow a population of (at least) 100 members for 100 generations in order to get a good fit provided the data are sufficiently accurate. Missing single pixels do not inhibit the parameter determination, as long as the key features are included in the data.

Since a typical restricted N-body simulation takes a few CPU-seconds on a Sparc workstation, a whole fitting procedure is finished after 3–6 CPU-hours.

In the third step the results of the previous steps are compared with detailed self-consistent N-body simulations. In the case of NGC4449 they show that the restricted N-body calculations are reliable models for this encounter. The comparison with the sticky particle models demonstrates that the HI gas can be modeled without any restriction by a purely stellar dynamical approach provided the encounter is as weak as in the case of NGC4449 and DDO125.

From the previous simulations I conclude that the extended HI features observed in NGC4449 are created by an encounter with DDO125. Prior to the encounter the HI gas formed an extended, almost homogenous disc with a large scale length of about 30 kpc and a radial extension of 40 ( $\pm 10$ ) kpc. The orientation of the disc is in agreement with the orientation of the inner ellipsoidal HI distribution. The orbital plane has an inclination angle of about  $40^\circ$  ( $\pm 10^\circ$ ). The eccentricity is close to that of a parabolic encounter ( $0.5 < \epsilon < 1.5$ ) and the apocenter distance of the galaxies is about 25 ( $\pm 5$ ) kpc. The closest approach happened  $3 - 4 \cdot 10^8$  yr ago. The mass ratio of both galaxies must be approximately 0.2 (and cannot be smaller than 0.1).

**Acknowledgements.** The simulations were partly performed with the GRAPE3af special purpose computer in Kiel (DFG Sp345/5). The author is grateful to Deidre Hunter, Jay Gallagher, Uli Klein, Sven Kohle and Hugo van Woerden for stimulating discussions about NGC4449. I am also greatly indebted to Konrad Kuijken and John Dubinski, who made their program for the generation of initial particle distributions available to the public, and Paul Charbonneau and Barry Knapp for providing their PIKAIA code. Last, but not least, I want to thank Joachim Köppen and Tim Freyer for a careful reading of the manuscript.

## References

- Arp H., 1966, *Atlas of peculiar galaxies*, Pasadena, Caltech (also ApJS, 14,1)  
Bäck Th., 1996, *Evolutionary Algorithms in Theory and Practice*, Oxford Univ. Press, Oxford  
Bajaja E., Huchtmeier W.K., Klein U., 1994, A&A, 285, 388  
Barnes J., 1988, ApJ, 331, 699  
Barnes J., Hernquist L., 1996, ApJ, 471, 115  
Barnes J., Hut P., 1986, Nature, 324, 446  
Bomans D., Chu Y.-H., 1997, AJ, 113, 1678  
Casoli F., Combes F., 1982, A&A, 110, 287  
della Ceca R., Griffiths R.E., Heckman T.M., 1997, ApJ, 485, 581  
Charbonneau P., 1995, ApJS, 101, 309  
Crillon R., Monnet G., 1969, A&A, 1, 449  
Ebneter K., Davis M., Jeske N., Stevens M., 1987, BAAS, 19, 681  
Fisher J.R., Tully R.B., 1981, ApJS, 47, 139  
Frenk C.S., White S.D.M., Davis M., Efstathiou G., 1988, ApJ, 327, 507  
Gerhard O., 1981, MNRAS, 197, 179



- Goldberg D.E., 1989, *Genetic Algorithms in Search, Optimization, & Machine Learning*, Addison-Wesley, Reading
- Hernquist L., 1987, ApJS, 64, 715
- Hernquist L., 1990, J. Comp. Phys., 87, 359
- Hernquist L., Katz N., 1989, ApJS, 70, 419
- Hernquist L., Ostriker J.P., 1992, ApJ, 386, 375
- Hill R.S., Home A.T., Smith A.M., Bruhweiler F.C., Cheng K.-P., Hintzen P.M., Oliverson R.J., 1994, ApJ, 430, 568
- Holland J., 1975, *Adaptation in natural and artificial systems*, Univ. of Michigan Press, Ann Arbor
- Holmberg E., 1941, ApJ, 94, 385
- Huang S., Carlberg R.G., 1997, ApJ, 480, 503
- Hunter D.A., Gallagher J.S., 1997, ApJ, 475, 65
- Hunter D.A., Gillet F.C., Gallagher J.S., Rice W.L., Low F.J., 1986, ApJ, 303, 171
- Hunter D.A., Thronson H.A., 1996, ApJ, 461, 202
- Hunter D.A., Wilcots E.M., van Woerden H., Gallagher J.S., Kohle S., 1998, ApJL, 495, L47
- Ibata R., Gilmore G., Irwin M., 1994, Nature, 370, 194
- Jungwiert B., 1997, private communication
- Kant I., 1755, in *Allgemeine Naturgeschichte und Theorie des Himmels oder Versuch von der Verfassung und dem mechanischen Ursprunge des ganzen Weltgebäudes nach Newtonischen Grundsätzen abgehandelt*, ed. H. Ebert, 1890, Verlag Wilhelm Engelmann, Leipzig
- Karachentsev I.D., Drozdovsky I.O., 1998, A&AS, 131, 1
- Klein U., Hummel E., Bomans D., Hopp U., 1996, A&A, 313, 396
- Kohle S., Klein U., Henkel C., Hunter D.A., 1998, in Proc. of *The Magellanic Clouds and Other Dwarf Galaxies*, ed. T. Richtler & J.M. Braun, Bad Honnef, see also [http://www.astro.uni-bonn.de/~webgk/ws98/skohle\\_p.html](http://www.astro.uni-bonn.de/~webgk/ws98/skohle_p.html)
- Kuijken K., Dubinski J., 1995, MNRAS, 277, 1341
- Noguchi M., 1988, A&A, 203, 259
- Palouš J., Jungwiert B., Kopecký J., 1993, A&A, 274, 189
- Pfleiderer J., Siedentopf H., 1961, Zs. f. Ap., 51, 201
- Press W.H., Teukolsky S.A., Vetterling W.T., Flannery B.P., 1992, *Numerical Recipes in FORTRAN - The Art of Scientific Computing*, Cambridge Univ. Press, Cambridge
- Quinn P.J., Hernquist L., Fullagar D.P., 1993, ApJ, 403, 74
- Rechenberg I., 1965, *Cybernetic solution path of an experimental problem*, Royal Aircraft Establishment, Library Translation No. 1122, Farnborough
- Rivolo A.V., Solomon P.M., 1987, in *Molecular Clouds in the Milky Way and External Galaxies*, ed. R. L. Dickman et al., Springer, p. 42
- Salo H., Laurikainen E., 1993, ApJ, 410, 586
- Sasaki M., Ohta K., Saito M., 1990, PASJ, 42, 361
- Schwefel H.-P., 1977, *Numerische Optimierung von Computer-Modellen mittels der Evolutionsstrategie*, Birkhäuser, Basel

- Sellwood J.A., 1980, A&A, 89, 296
- Silk J., Wyse R.F.G., Shields G.A., 1987, ApJ, 322, L59
- Sugimoto D., Chikada Y., Makino J., Ito T., Ebisuzaki T., Umemura M., 1990, Nature, 345, 33
- Theis Ch., Hensler G., 1993, A&A, 280, 85
- Theis Ch., Kohle S., 1998, in Proc. of *The Magellanic Clouds and Other Dwarf Galaxies*, ed. T. Richtler & J.M. Braun, Bad Honnef, see also [http://www.astro.uni-bonn.de/~webgk/ws98/ctheis\\_t.html](http://www.astro.uni-bonn.de/~webgk/ws98/ctheis_t.html)
- Thomasson M., Donner K.J., 1993, A&A, 272, 153
- Tóth G., Ostriker J.P., 1992, ApJ, 389, 5
- Toomre A., 1977, in *The Evolution of Galaxies and Stellar Populations*, ed. B.M. Tinsley & R.B. Larson, Yale Univ. Obs. New Haven
- Toomre A., Toomre J., 1972, ApJ, 178, 623
- Tully R.B., Bottinelli L., Fisher J.R., Gouguenheim L., Sancisi R., van Woerden H., 1978, A&A, 63, 37
- van Woerden H., Bosma A., Mebold U., 1975, in *La Dynamique des Galaxies Spirales*, ed. L. Weliachew, p. 483
- Velázquez H., White S.D.M., 1998, preprint, astro-ph/9809412
- Vorontsov-Velyaminov B.A., 1959, *Atlas and Catalog of Interacting Galaxies*, Moscow, Sternberg Institute
- Wahde M., 1998, A&AS, 132, 417
- Walker I.R., Mihos J.C., Hernquist L., 1996, ApJ, 460, 121
- White S.D.M., 1978, MNRAS, 184, 185

This figure "fig1.gif" is available in "gif" format from:

<http://arxiv.org/ps/astro-ph/9907237v1>

This figure "fig2.gif" is available in "gif" format from:

<http://arxiv.org/ps/astro-ph/9907237v1>

This figure "fig3.gif" is available in "gif" format from:

<http://arxiv.org/ps/astro-ph/9907237v1>

This figure "fig4.gif" is available in "gif" format from:

<http://arxiv.org/ps/astro-ph/9907237v1>

This figure "fig5.gif" is available in "gif" format from:

<http://arxiv.org/ps/astro-ph/9907237v1>

This figure "fig6.gif" is available in "gif" format from:

<http://arxiv.org/ps/astro-ph/9907237v1>



This figure "fig7.gif" is available in "gif" format from:

<http://arxiv.org/ps/astro-ph/9907237v1>

This figure "fig8.gif" is available in "gif" format from:

<http://arxiv.org/ps/astro-ph/9907237v1>

This figure "fig9.gif" is available in "gif" format from:

<http://arxiv.org/ps/astro-ph/9907237v1>

This figure "fig13.gif" is available in "gif" format from:

<http://arxiv.org/ps/astro-ph/9907237v1>

This figure "fig14.gif" is available in "gif" format from:

<http://arxiv.org/ps/astro-ph/9907237v1>

This figure "fig15.gif" is available in "gif" format from:

<http://arxiv.org/ps/astro-ph/9907237v1>

This figure "fig16.gif" is available in "gif" format from:

<http://arxiv.org/ps/astro-ph/9907237v1>

This figure "fig17.gif" is available in "gif" format from:

<http://arxiv.org/ps/astro-ph/9907237v1>



This figure "fig18.gif" is available in "gif" format from:

<http://arxiv.org/ps/astro-ph/9907237v1>